Deep-Sea Research Part I 144 (2019) 28–38

Contents lists available at ScienceDirect

Deep-Sea Research Part I

journal homepage: www.elsevier.com/locate/dsri

The impact of sea ice on the air-sea exchange of mercury in the Arctic Ocean

Brian P. DiMento[a,*], Robert P. Mason[a], Steven Brooks[b], Chris Moore[c]

[a] Department of Marine Sciences, University of Connecticut, 1080 Shennecossett Rd, Groton, CT 06340, USA
[b] Department of Mechanical, Aerospace and Biomedical Engineering, University of Tennessee Space Institute, Tullahoma, TN 37388, USA
[c] Gas Technology Institute, Des Plaines, IL 60013, USA

ARTICLE INFO

Keywords:
Mercury
Elemental mercury
Methylmercury
Gas evasion
Air-sea exchange
Aerosols
Precipitation
Snow
Ice
Arctic

ABSTRACT

Atmospheric deposition is the main input of mercury (Hg) to the ocean, even in remote locations such as the Arctic. Furthermore, evasion of elemental Hg (Hg^0) is the major sink for oceanic Hg. As a result, air-sea exchange is an important part of the oceanic Hg cycle. To examine the air-sea exchange of Hg in the Arctic Ocean we made high resolution measurements of Hg^0 in surface waters and Hg speciation in the atmosphere using continuous sampling systems during the 2015 U.S. Arctic GEOTRACES cruise from August 9 to October 12. Additionally, samples were obtained for measurement of total Hg and methylmercury (CH_3Hg) in wet deposition and bulk aerosols as well as surface snow and sea ice. We used these measurements made in the water and the atmosphere to estimate fluxes of Hg^0 from the ocean to the atmosphere. Concentrations of dissolved Hg^0 (Hg^0_{diss}) were near saturation in ice-free waters (32 ± 30 fM) and resultant fluxes were low; however, Hg^0 was highly enriched under contiguous ice (101 ± 98 fM, up to 544 fM) suggesting the continual formation of Hg^0 in waters even when ice covered. Predicted evasion fluxes in these regions (these being potential rates for locations under ice) were as high as 492 pmol m^{-2} h^{-1}. Atmospheric Hg^0 concentrations averaged 1.2 ± 0.1 ng m^{-3} with little variation over the course of the cruise even above waters with elevated Hg^0_{diss}, indicating that sea ice acts as a barrier to air-sea exchange. Measurements of Hg in precipitation and aerosols were lower than have been found in more coastal regions of the Arctic. We used these concentrations to estimate deposition of Hg and CH_3Hg during the time of the cruise. Overall, wet deposition represented 88% of the CH_3Hg flux and 38% of the Hg_T flux. Our flux estimates confirm the importance of air-sea exchange in Hg cycling in the Arctic and suggest that evasion was greater than deposition, indicating a net loss of Hg from the Arctic during this period or the presence of other sources not measured during this study. Additionally, our results suggest that fluxes for offshore waters are lower than found in coastal regions of the Arctic. From these estimates, we predict how Hg concentrations may respond to future changes in ice cover and other potential impacts of climate change on Hg dynamics and food web bioaccumulation in this important ocean region.

1. Introduction

Mercury (Hg), a global contaminant, is of significant interest in the Arctic due to its toxicity and presence in an environment far removed from sources of anthropogenic emissions. Elevated Hg concentrations in Arctic biota are believed to largely be derived from atmospheric deposition (AMAP, 2011), which has increased in remote locations threefold since pre-industrial times (Kirk et al., 2012; Lindberg et al., 2007). Riverine discharge, thawing permafrost, coastal erosion, and oceanic circulation have also played a role in the transport of Hg to the Arctic marine environment (AMAP, 2011; Fisher et al., 2012; Zhang et al., 2015). A long residence time (6–12 months) in the atmosphere results in the transport of elemental mercury (Hg^0) over long distances from various natural and anthropogenic sources at lower latitudes, including coal combustion and other industrial processes (Corbitt et al., 2011; Slemr et al., 1985). This long-range transport and the remote location of the Arctic make the attribution and quantification of sources of Hg to the polar region more difficult.

The Arctic is uniquely differentiated from other marine ecosystems by its extensive continental shelf (~ 50% of the Arctic Ocean surface area), and large freshwater inputs from ice melt and river runoff that result in salinity driven stratification of the surface mixed layer. These features, along with its remote location and unique seasonal atmospheric events, can affect the fate and distribution of Hg and

Abbreviations: Hg^0_{diss}, dissolved elemental mercury; Hg^0_{atmos}, atmospheric elemental mercury; CH_3Hg, methylmercury; Hg_T, total mercury; Hg_R, reactive gaseous mercury; Hg_P/CH_3Hg_P, particulate aerosol mercury/methylmercury; Hg_{oxid}, total oxidized mercury; MIZ, marginal ice zone

* Corresponding author.
E-mail address: brian.dimento@uconn.edu (B.P. DiMento).

https://doi.org/10.1016/j.dsr.2018.12.001
Received 6 June 2018; Received in revised form 4 October 2018; Accepted 1 December 2018
Available online 03 December 2018
0967-0637/

methylmercury (CH_3Hg) and thus its potential accumulation and impact on humans who rely on Arctic marine mammals and fish for subsistence (AMAP, 2011). Concerns raised over the health of these indigenous people and the animals they consume from CH_3Hg exposure has resulted in major research initiatives undertaken to help understand the transport, transformation, and biological uptake of Hg and CH_3Hg in the Arctic marine ecosystem.

Ice cover on a large portion of the Arctic Ocean for much of the year impacts Hg air-sea exchange as well as photochemical processes, in addition to creating challenging conditions for sampling. The transitional region between open water and contiguous sea ice, the marginal ice zone (MIZ), has also been shown to play an important role in the accumulation of CH_3Hg in the water column (Heimbürger et al., 2015). A warming climate has resulted in dramatic changes to the vast sea-ice environment in the Arctic over the past decades (Macdonald et al., 2005). Temperatures in the Arctic have risen at a rate nearly twice that of the global average (Bekryaev et al., 2010; Bintanja et al., 2011; Screen and Simmonds, 2010), resulting in a 5–10% decrease per decade in annual mean sea ice extent in many regions of the Arctic (Cavalieri and Parkinson, 2012; Parkinson and Cavalieri, 2008). The biogeochemical cycling of Hg is expected to be sensitive to the rapid changes taking place in the region in recent decades (Macdonald et al., 2005; Stern et al., 2012). An increase in Hg^0 evasion would be expected due to both higher temperatures and lower ice cover, with further enhancement by increased net photochemical Hg(II) reduction under greater ultraviolet radiation, a result of increased Arctic ozone depletion (Bais et al., 2011; O'Driscoll et al., 2006). Climate positive feedback loops will further enhance these processes.

Air-sea exchange is a critical part of the global Hg cycle, including in the Arctic Ocean. Changes in the Arctic ecosystem, resulting in alterations in Hg inputs, have increasingly driven highly variable CH_3Hg concentrations in upper trophic-level marine biota in recent decades. These changes are greater than would be expected from external anthropogenic emissions alone (Chaulk et al., 2011; Macdonald et al., 2005; Outridge et al., 2008; Stern et al., 2012; Wang et al., 2010). Wet and dry deposition are the dominant sources of Hg to the global oceans, accounting for 70% or more of the inputs, while gas evasion is the dominant sink, accounting for about 90% of the outputs (Driscoll et al., 2013; Fitzgerald et al., 2007; Lamborg et al., 2014; Mason et al., 2012). Springtime atmospheric mercury depletion events (AMDE) due to Hg^0 oxidation by bromine (Br) and BrO radicals result in the increased deposition of the water soluble divalent Hg(II) species (Ariya et al., 2004; Schroeder et al., 1998; Steffen et al., 2008). While AMDEs are most pronounced in spring they can occur at other times of the year in polar regions (Nerentorp Mastromonaco et al., 2016) and are not only confined to such locations (Brunke et al., 2010). Other studies have shown that photochemical reduction in the surface ocean and snowpack results in the evasion of approximately half of the deposited Hg (Dastoor et al., 2015; Kirk et al., 2006; Lalonde et al., 2002; Soerensen et al., 2016; Strode et al., 2007). These events control the magnitude and timing of Hg flux into the aquatic ecosystem, where it can then be transformed to CH_3Hg and accumulated into biota, reemitted as Hg^0, or trapped under the ice.

Recycling of Hg in the surface ocean through redox reactions and air-sea exchange extends the response time of Hg to changes in(anthropogenic inputs. CH_3Hg concentrations are indirectly impacted due to the effects of deposition and evasion on total Hg (Hg_T) concentrations. Elevated CH_3Hg concentrations found in Arctic fish and marine mammals are likely a result of a combination of increased deposition as well as enhanced biomagnification resulting from climate-driven shifts in ecosystem characteristics and trophic structure (Braune et al., 2015; Clarkson and Magos, 2006; Mahaffey et al., 2011; Stern et al., 2012). Therefore, in order to accurately predict the response of oceanic Hg_T and CH_3Hg concentrations to changing anthropogenic inputs and a warming climate, we need to develop a comprehensive understanding of the factors affecting Hg^0 gas exchange at the ocean surface.

With the exception of the Arctic Ocean, high resolution measurements of Hg^0_{diss} in surface waters have revealed relatively consistent concentrations within a geographic region (Andersson et al., 2008a, 2008c; Kuss et al., 2011; Mason et al., 2017; Soerensen et al., 2014, 2013). In regions such as the western North Atlantic, Hg inputs were determined to be a potential driver of differences in Hg^0_{diss} concentrations when moving from the continental shelf to offshore waters (Soerensen et al., 2013). In the Arctic, in addition to waters influenced by river discharge, ice covered regions were also found to have higher Hg^0_{diss} concentrations (Andersson et al., 2008c). This trend was also observed in the Antarctic (Nerentorp Mastromonaco et al., 2017a, 2017b). Evasion of this Hg^0 also contributes to elevated levels in the atmospheric boundary layer (Soerensen et al., 2010; Steffen et al., 2015; Strode et al., 2007). While modeling efforts suggest a drastic increase in Hg^0 evasion since the pre-industrial era, flux calculations often rely on short term measurements and thus might not reflect yearly averages (e.g., Mason et al., 1998). More data is therefore required to further constrain such estimates, especially in the Arctic where interannual variability has been greater than any long term trends observed since Hg^0 monitoring started (Fisher et al., 2013; Steffen et al., 2008).

Understanding Hg speciation, transformations, and air-sea exchange in Arctic waters is crucial to determining the factors controlling the ultimate bioaccumulation of CH_3Hg in marine food webs. The objective of this study was therefore to improve our knowledge of Hg air-sea exchange in the Arctic through measurements in surface waters as well as the atmospheric boundary layer. Based on limited previous data in the Arctic, we hypothesized that the concentration of Hg^0_{diss} would be positively correlated with sea ice coverage due to the hindrance of evasion. We also predicted that Hg^0 concentrations and evasional fluxes would be lower away from riverine inputs, with biological processes promoting the oxidation of Hg^0_{diss} and facilitating its removal by particle settling in waters along the continental shelf. Using measurements of CH_3Hg and Hg_T in precipitation and aerosols, we estimated the Hg inputs from the atmosphere to the surface ocean, and contrasted these with calculated gas evasion fluxes. Finally, we compared our results with measurements made in other regions as well as previous attempts to model Hg cycling within the Arctic.

2. Materials and methods

2.1. Sampling methods

Simultaneous atmospheric Hg^0 (Hg^0_{atmos}) and Hg^0_{diss} measurements (five minute temporal resolution) were made aboard the United States Coast Guard Cutter (USCGC) *Healy* on the U.S. GEOTRACES Arctic (GN01) cruise in the Western Arctic Ocean from August 9, 2015 to October 12, 2015, from Dutch Harbor, Alaska to the North Pole and back. The cruise proceeded northward along the western leg of the track (~180°W) through the Bering Strait and across the Makarov Basin, and returned southward along the eastern leg (~150°W) across the Canada Basin (Fig. 1). All figures of underway data, collected while the ship was in motion (i.e., traveling between stations), are plotted with the western leg of the cruise on the left and the eastern return leg of the cruise on the right. The marginal ice zone (MIZ), the transition between open ocean and sea ice, was found from 73.5° to 81°N on the western leg and 79–77.5°N on the eastern leg, with contiguous ice in between (81–90–79°N).

Atmospheric Hg measurements in the marine boundary layer were made using the suite of Tekran modules (2537A/1130/1135) for the determination of Hg^0, reactive gaseous Hg (Hg_R), fine particulate Hg (Hg_{PF}), and total oxidized Hg (Hg_{oxid}) using methods described in the literature (Gichuki and Mason, 2014; Landis et al., 2002; Laurier et al., 2003; Lindberg et al., 2001). The latter of these species are operationally defined based on their methods of analysis. Air enters the analyzer through an elutriator that removes aerosols < 2.5 μm that would deposit onto the denuder walls if not removed (Landis et al.,

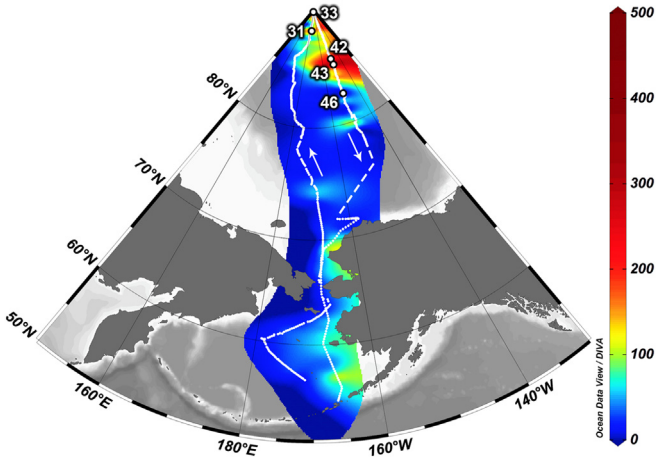

Fig. 1. The U.S. Arctic GEOTRACES cruise track and dissolved Hg° ($Hg°_{diss}$) concentrations (fM). The cruise track is represented in white, with the dashed line on the eastern leg of the cruise representing the section where underway data collection was stopped. The numbered locations are the stations where ice cores were taken. $Hg°_{diss}$ data interpolation was done using the Data-Interpolating Variational Analysis (DIVA) software tool in Ocean Data View (Schlitzer, 2015).

2002). Thus, particulate concentrations determined by the Tekran speciation system do not represent the bulk aerosol but only the fine fraction. The sampling inlet was located on the bow of the ship at a height of 9.5 m above sea level. After the initial instrument external calibration, manual injections were repeated twice weekly to check the calibration. Internal calibrations were repeated every 26 h to the system so it was calibrated at different times every other day. The detection limit for Tekran 2537 A ($Hg°_{atmos}$) unit is < 0.1 ng m^{-3}, as reported by Tekran (2005). Detection limits for the speciation units (Tekran 1130 and 1135), calculated from the standard deviation of field blank replicates (Landis et al., 2002), were 1.0 pg m^{-3} Hg_R and Hg_{PF}, and 3.5 pg m^{-3} Hg_{oxid}. Additional analytical details are included in the Supporting information.

$Hg°_{diss}$ concentrations were determined using a continuous equilibrium system (Andersson et al., 2008a; Mason et al., 2017; Soerensen et al., 2014), which was developed to make high resolution measurements underway using the ship's seawater intake at 7 m depth. Briefly, the opposite flow principle was used to establish a continuous equilibrium between the aqueous and gaseous phases by exchanging Hg° from the water into counter-flowing air, introduced as bubbles by sparging. The gaseous Hg° in the air equilibrated with the aqueous phase was dried prior to entering the Tekran. The measured Hg° concentration in the outgoing gas ($[Hg°_{gas}]$) is equivalent to the $Hg°_{diss}$ concentration multiplied by the dimensionless Henry's Law constant ($k_{H'}$) at the current temperature and salinity of the water.

$$[Hg°0_{diss}] = [Hg°0_{gas}]/k_H \quad (1)$$

This method can measure both $Hg°_{diss}$ and dimethylmercury ($(CH_3)_2Hg$), but measurements of $(CH_3)_2Hg$ made aboard the ship (K. Bowman and A. Agather, personal commun.) indicate that it represented only a small fraction ($< 5\%$) of the total dissolved gaseous Hg in the surface waters. Therefore, the measurements were assumed to reflect the concentrations of $Hg°_{diss}$. In this paper, concentrations (and fluxes) of dissolved Hg are reported in molar units (100 fM ≈ 20 pg L^{-1}) while atmospheric measurements are reported in mass units to remain consistent with conventions in the literature.

The same intake used for the $Hg°_{diss}$ measurements was also used to continuously (every 15 s) determine surface temperature, salinity, and fluorescence. These ancillary data, along with other supplementary data (Fig. S1–8), are shown in the Supporting information. Along with wind speed and Hg_{eq} measurements, these data were averaged into hourly values before calculating $Hg°_{diss}$ concentrations and gas exchange parameters. Due to concerns of contamination when the ship was stationary, data collected while the ship was on station were removed from the underway $Hg°_{diss}$ measurements plotted in the figures. As was the case on the previous GEOTRACES cruises, these data were not used in the flux calculations (Mason et al., 2017). Generally, the $Hg°_{diss}$ concentrations while the ship was on station were higher than while underway.

An automated N-CON rain sampler (designated for Hg analysis) was used to collect rain (falling snow was not collected for Hg analysis) during the cruise. It was arranged and operated to avoid contamination from the ship and sea spray, only opening for collection during a rain event (Mason et al., 2017). Low rainfall warranted ultra high purity water rinses of the collection funnel in all but one sample, with the rinse and sample combined and recovered for analysis. Two deployment blanks were also analyzed and subtracted from rainwater sample concentrations.

Fourteen bulk aerosol deployments were made over periods of three to five days using high-volume aerosol samplers following methods in Morton et al. (2013). During each deployment, aerosol samples were collected in triplicate on pre-combusted glass-fiber (GFF) or quartz fiber (QMA) filters. Unused filters were set aside for blank analyses. Sampling duration lasted an average of 31.0 h (11.0–80.0 h) with an average volume filtered of 172.5 m^3 (60.6–451.9 m^3). Both aerosol and rain samplers were deployed directly above the bridge, about 23 m from the waterline, to help minimize contamination. Additional aerosol deployment details can be found in Marsay et al. (2018b).

Ice cores were sampled using a trace metal clean corer at five stations, with duplicate cores collected at two of the five locations. Ice stations were located between 88.4°N on the western leg and 82.5°N on the eastern leg of the cruise. Whole ice cores were returned to the Hg clean facility where colleagues on the ship subsampled them into sections. Once the cores were divided, the subsections were placed in Teflon collection containers and defrosted under trace metal clean conditions. The samples were then decanted into Teflon bottles and refrozen. The collection containers were cleaned and re-used for the next ice core. Cores did not extend to the bottom of the sea ice because of the concern that the samples would not be representative of the ice itself due to infiltration of seawater during coring. Porous ice also potentially resulted in the loss of brine waters within the core during sampling.

Triplicate bulk snow samples were collected at the same sites as the ice cores. Snow was collected using an acid cleaned HDPE shovel, and transported in a LDPE container before being melted and subsampled on board. Melt pond samples were also collected at these five ice stations using a peristaltic pump with acid-cleaned tubing. Additional ice, snow, and melt pond sampling details can be found in Marsay et al. (2018a).

After collection, snow and ice samples were melted and transferred to acid-cleaned glass bottles (I-CHEM Certified 200 series), and precipitation samples were stored in Teflon FEP bottles. Aerosol filters were stored in acid cleaned polystyrene petri dishes. All samples were kept frozen at −20 °C in the dark, and were transported back to the University of Connecticut for analysis.

2.2. Analytical methods

Methylmercury concentrations were determined following the ascorbic acid-assisted direct ethylation method (Munson et al., 2014) using a Tekran 2700 instrument and autosampler to automate the purging, trapping, and detection via cold vapor atomic fluorescence spectroscopy (CVAFS). Samples were thawed then acidified to 1% (v/v) H_2SO_4 to digest overnight before neutralizing with potassium hydroxide (KOH), buffering with acetate buffer,(adding ascorbic acid and finally sodium tetraethyl borate (NaTEB) to(ethylate the CH_3Hg. Sample concentrations were corrected (for matrix spike recoveries,

which averaged 82% with a typical relative standard(deviation (RSD) of 10%. Average method detection limits (MDL) were < 10 fM.

Total mercury concentrations were determined by dual gold-amalgamation CVAFS utilizing a Tekran 2600 instrument in accordance with U.S. EPA Method 1631 (Lamborg et al., 2012; U.S. Environmental Protection Agency, 2002). Briefly, waters were digested with bromine monochloride (BrCl) followed by a pre-reduction step with hydroxylamine hydrochloride ($NH_2OH{\cdot}HCl$). Inorganic Hg(II) was then reduced to Hg° using stannous chloride ($SnCl_2$) prior to automated analysis on the Tekran. Matrix spike recoveries averaged 98 ± 9%, and the MDL was 0.25 pM.

Aerosol filters were digested in acid-cleaned 15-mL centrifuge tubes with 10 mL of 4.57 M trace metal grade HNO_3, placed in a covered 60 °C water bath for 12 h (Hammerschmidt and Fitzgerald, 2006, 2005). A subsample of this digest was taken for particulate bulk aerosol CH_3Hg (CH_3Hg_{PB}) analysis, and the remainder was further digested with BrCl overnight at room temperature for total Hg (Hg_{PB}) analysis. Method detection limits were ~ 0.1 pg m^{-3} for Hg_{PB} and 2 fg m^{-3} for CH_3Hg_{PB}, based on the average volume of air filtered and the volume of digest analyzed.

2.3. Hg° concentration and flux calculations

Flux calculations were performed following the approach of Soerensen et al. (2010) and Mason et al. (2017). The Hg° flux (F, reported in units of pmol m^{-2} h^{-1}) is defined as follows:

$$F = k_w([Hg°0_{diss}] - [Hg°0_{atmos}]/ k_H,) \quad (2)$$

where k_w (m h^{-1}) is the water side mass transfer coefficient (gas-transfer velocity), $[Hg°_{diss}]$ (ng m^{-3}) is the concentration of Hg° in water, and $[Hg°_{atmos}]$ (ng m^{-3}) is the concentration of Hg° in air. The mass transfer coefficient (k_w) is calculated from the wind speed and Schmidt number for Hg and CO_2, which is equal to the ratio between the kinematic viscosity of the water and the aqueous diffusivity of Hg (Andersson et al., 2008b). Positive fluxes represent evasion out of the ocean to the atmosphere, while negative fluxes are into the ocean. The degree of saturation (S) is defined as:

$$S = [Hg°0_{diss}]/[Hg°0_{diss}]_{eq} *100 \text{ where} [Hg°0_{diss}]_{eq} = [Hg°0_{atmos}]/k_H, \quad (3)$$

where $[Hg°_{diss}]_{eq}$ represents the concentration of Hg° in equilibrium with the air.

Wet and dry deposition were estimated using the concentration of Hg in precipitation and aerosols, along with the Hg_R concentration, using the parameters summarized in Soerensen et al. (2016). Wet deposition is calculated by the Hg concentration multiplied by the annual rain/snow fall, while the dry particulate deposition flux is equal to the product of the measured aerosol and Hg_R concentrations and the dry deposition velocity (Mason et al., 2017). Because Hg_R values are expected to show significant seasonal variation due to substantial Hg_R formation during Hg depletion events in the spring (Lindberg et al., 2001), flux values were calculated on a per month basis and were not extrapolated to an annual flux.

3. Results

3.1. Trends in dissolved Hg

Trends in $Hg°_{diss}$ concentration in the Arctic Ocean (Fig. 2) will be discussed in terms of three geographical regions – contiguous ice (81 – 90 – 79°N), the MIZ (73.5 – 81°N, 79 – 77.5°N), and open water (south of the MIZ). The overall average hourly concentration of $Hg°_{diss}$ was 68 ± 83 fM, ranging from 3.9 to 454 fM. In open water, the average concentration was 32 ± 30 fM, while under contiguous ice the average was significantly higher ($p < 0.0001$), 101 ± 98 fM, reaching a maximum instantaneous value of 544 fM under the contiguous ice.

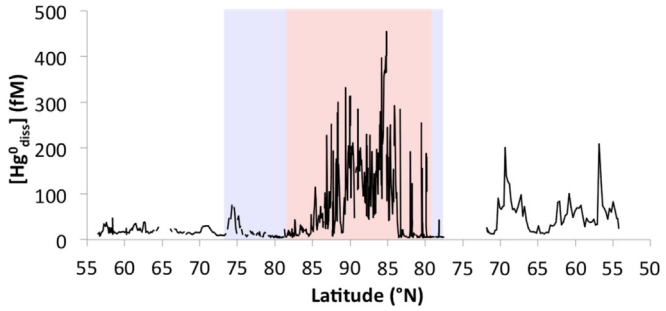

Fig. 2. Dissolved Hg° ($Hg°_{diss}$) concentrations, averaged hourly, along the U.S. Arctic GEOTRACES cruise track during the marginal ice (light blue shading; 73.5–81°N, 79–77.5°N) and contiguous ice (pink shading; 81–90–79°N) zones. (For interpretation of the references to color in this figure legend, the reader is referred to the web version of this article).

Concentrations were elevated near shore on the eastern return leg of the cruise suggesting increased coastal inputs or a change in water circulation during the duration of the cruise.

3.2. Trends in atmospheric Hg

Variability in atmospheric Hg° concentrations in the marine boundary layer was much lower than sea surface $Hg°_{diss}$ concentrations. Average hourly $Hg°_{atmos}$ concentrations (Fig. 3) ranged from 0.86 to 1.88 ng m^{-3}, with an average of 1.25 ± 0.10 ng m^{-3} (Table 2). The highest concentrations were observed in the Bering Sea at the start of the cruise and in the Bering Strait on the return leg. Following a brief significant ($p < 0.0001$) drop in Hg° from 73.5° to 77°N (1.15 ± 0.11 ng m^{-3} vs. 1.25 ± 0.04 ng m^{-3}) after entering the MIZ, concentrations briefly rose ($p < 0.0001$) later in the MIZ (77–81°N; 1.34 ± 0.11 ng m^{-3}) before slowly returning to average values over the continuous ice zone.

Concentrations of Hg_R and Hg_{PF} measured by the Tekran speciation units were very low, averaging 1.7 pg m^{-3} and 2.2 pg m^{-3}, only about two times greater than the detection limit for each species. Particulate bulk aerosol CH_3Hg_{PB} and total Hg_{PB} concentrations (Fig. S3) measured on filters were generally low, with many measurements below the method detection limit. Average CH_3Hg_{PB} concentrations were 1.4 ± 1.9 fg m^{-3}, while Hg_{PB} averaged 0.33 ± 0.34 pg m^{-3} (Table 1). The similarity between the values of Hg_{PF} and Hg_{PB} indicates that most of the Hg was in the fine fraction of the aerosol phase and not associated with larger particles, which would predominantly be sea salt in the Arctic. The percent CH_3Hg in the aerosol was 0.5 ± 0.5%, lower than was found in precipitation.

The concentration of Hg_{oxid} measured by the total pyrolyzer averaged 6.9 pg m^{-3}. This value should be equivalent to Hg_R + Hg_{PB}, and again, given the low values found on the cruise, the values are comparable. The low values for both the aerosol and the Hg_R are an indication that dry deposition is not an important atmospheric sink of Hg

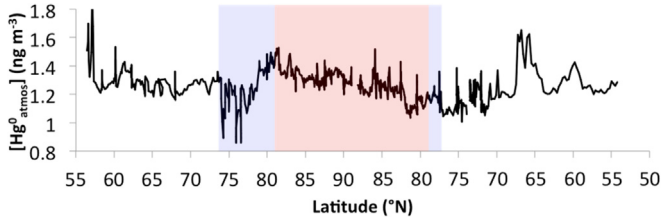

Fig. 3. Underway atmospheric Hg° concentrations ($[Hg°_{atmos}]$) along the U.S. Arctic GEOTRACES cruise track during the marginal ice (light blue shading; 73.5–81°N, 79–77.5°N) and contiguous ice (pink shading; 81–90–79°N) zones. (For interpretation of the references to color in this figure legend, the reader is referred to the web version of this article).

Table 1
Summary of average methyl (CH_3Hg) and total Hg (Hg_T) concentrations, in addition to percent CH_3Hg, in atmospheric bulk aerosols and precipitation samples, as well as ice cores, snow and melt pond water on the surface of sea ice.

	[CH_3Hg]	[Hg_T]	%CH_3Hg
Bulk Aerosols	1.4 ± 1.9 fg m^{-3}	0.33 ± 0.34 pg m^{-3}	0.53 ± 0.50%
Precipitation	33 ± 28 fM	3.1 ± 2.1 pM	1.2 ± 0.64%
Snow	11 ± 1 fM	3.6 ± 1.3 pM	0.41 ± 0.49%
Melt Pond	97 ± 75 fM	11 ± 9 pM	1.3 ± 0.8%
Ice Cores	86 ± 120 fM	2.8 ± 2.0 pM	3.5 ± 4.3%

in this region during the time of the cruise.

3.3. Hg in precipitation

Rain collected during this cruise had an average CH_3Hg concentration of 0.033 ± 0.028 pM and a Hg_T concentration of 3.1 ± 2.1 pM, with a % CH_3Hg of 1.2 ± 0.6% (Table 1). Most rain events were small with minimal or trace amounts of precipitation collected. Concentrations were variable with no observed strong geographic trends for both rain and aerosols (Fig. S3, S4).

3.4. Ice cores, surface snow and melt ponds

CH_3Hg and Hg_T profiles from ice cores at the five stations sampled are shown in Fig. 4. Higher concentrations were generally found at the surface, decreasing with depth in the core. Percent CH_3Hg was highly variable, averaging 3.5 ± 4.3% (Table 1), with peak values often observed at the base of the core. No latitudinal trend was observed in concentration or % CH_3Hg.

Falling snow was not collected for Hg analysis during this cruise, but surface snow on ice sheets was collected at ice stations. Average concentrations in snow (Table 1) were 11 ± 1 fM CH_3Hg and 3.6 ± 1.3 pM Hg_T. In melt pond waters, CH_3Hg averaged 97 ± 75 fM and Hg_T 11 ± 9 pM.

4. Discussion

4.1. Trends in Hg°_{diss}

Trends in Hg°_{diss} concentrations indicated that ice cover acted as a barrier to Hg evasion. Concentrations measured in open water during the early part of the cruise (19 ± 7 fM) were generally lower than earlier studies in the region (Andersson et al., 2008c; Kim et al., 2016). Higher concentrations (74 ± 18 fM) were measured in July by Kim et al. (2016) further south in the Bering Sea, as well as by Andersson et al. (2008c) in the Chukchi Sea (100–300 fM) in late July and early August. These elevated levels were encountered further south than in our study, possibly because of the earlier timing of their cruise following ice-out. Kirk et al. (2008) also measured Hg°_{diss} during the same time of the year in surface waters of the CAA and Hudson bay, and found concentrations of 127 ± 51 fM and 148 ± 25 fM, respectively.

Early in the cruise there was some evidence for a diurnal change in Hg°_{diss} concentrations (Fig. S7). This trend has been observed before, but only in coastal waters (e.g., Amyot et al., 1994, 1997; Andersson et al., 2007; Tseng et al., 2013). Diurnal variability was not observed later in the cruise after leaving the continental shelf, likely due to the greater depths and the presence of sea ice, along with the increased variability in concentrations. Potential correlations between Hg° concentrations and other variables during the early part of the cruise are discussed in the SI (Fig. S8).

Entering the MIZ, aside from a brief peak in Hg°_{diss}, concentrations did not immediately begin to rise, indicating a lag between ice cover and elevated concentrations. There was no significant change in concentration between the period of open water before the MIZ and the MIZ on the western (northern) transect of the cruise ($p > 0.05$). Concentrations peaked under contiguous the ice, but did not reach as high of values as were measured by Andersson et al. (2008c) (544 vs. 670 fM). This maximum was observed south of the pole along the eastern return leg of the cruise, 17 times higher than observed on average in the open water, in a location that generally corresponded with a greater concentration of multi-year ice (NOAA Climate.gov, 2016) (Fig. 5).

Variability in Hg°_{diss} concentrations was high under the ice, possibly

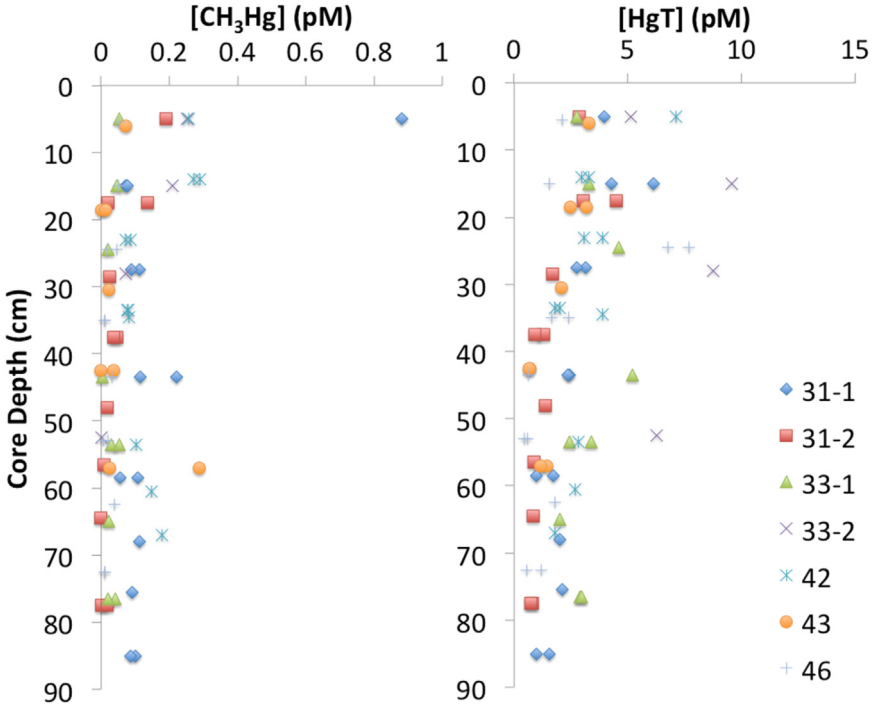

Fig. 4. Methyl (CH_3Hg) and total Hg (Hg_T) concentrations in ice cores taken during the U.S. Arctic GEOTRACES cruise.

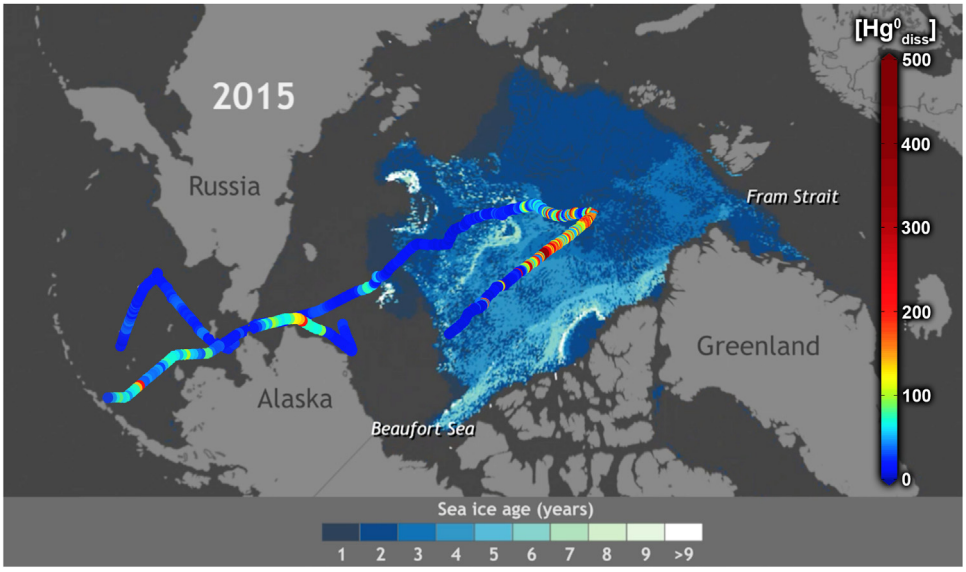

Fig. 5. The dissolved Hg° concentrations (fM) along the U.S. Arctic GEOTRACES cruise track overlaid on ice coverage in the Arctic during September 2015 (NOAA Climate.gov, 2016, based on data from Tschudi et al., 2016).

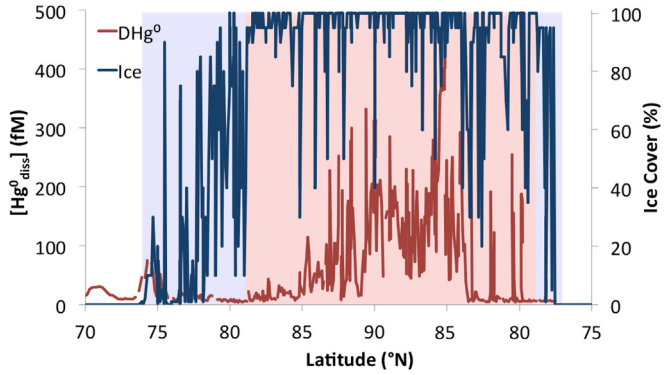

Fig. 6. The dissolved Hg° (Hg°_{diss}) concentration along the U.S. Arctic GEOTRACES cruise track during the marginal ice (light blue shading; 73.5–81°N, 79–77.5°N) and contiguous ice (pink shading; 81–90–79°N) zones. (For interpretation of the references to color in this figure legend, the reader is referred to the web version of this article).

due to varying extent and duration of ice cover. The presence or absence of leads and open water, both prior to and at the time of sampling, could have contributed to this variability. As shown in Fig. 6, peaks in Hg°_{diss} generally occur in regions with near-complete ice cover, indicating that degassing in open leads could have resulted in the local drops in concentration. Photochemical oxidation of Hg° could also be enhanced in regions with open leads or minimal ice cover due to increased light exposure in surface waters (Amyot et al., 1997). Despite the observed variability in the contiguous ice zone, there was still a significant ($p = 0.004$) positive relationship between Hg°_{diss} concentrations and ice cover.

Additional variability in underway data could have been due to the movement of the ship, breaking through the ice and mixing the surface water as it finds its way and creates openings in the ice. However, a study of ^{222}Rn concentrations concluded, based on measurements collected from a ship on station and from locations removed from the ship's influence (sampled through ice), that there was no impact of the ship on the ^{222}Rn concentration and profile within the surface mixed layer (Rutgers van der Loeff et al., 2014). Also, at stations under ice, the ^{222}Rn concentrations were close to secular equilibrium suggesting that gas exchange had not occurred to any substantial degree over the timescale needed to reach secular equilibrium (several weeks). While no ^{222}Rn measurements were made while the ship was underway, the results do overall suggest that the large variations found in the Hg°_{diss} cannot be attributed solely to the ship's movement, ice breaking and associated mixing.

Additionally, the ^{222}Rn data also suggest limited gas exchange in regions with ice cover (Rutgers van der Loeff et al., 2014), which is consistent with the conclusions of Loose et al. (2011) but contrary to the conclusions of others (e.g., Fanning and Torres, 1991). There is an ongoing debate on the potential for gas exchange in ice-covered regions with leads and other breaks in the ice. The Rutgers van der Loeff et al. (2014) data suggest that the rate of gas exchange in regions with partial ice cover were less than would be predicted based on estimations assuming gas exchange was happening normally in open waters between ice. This is contrary to lab experiments that indicated that gas exchange was enhanced over prediction in partial ice covered waters (Loose et al., 2009). We found no evidence for enhanced gas exchange (i.e. Hg°_{diss} depletion) at the ice edge stations. The variability under the ice with maximum concentrations falling between drops in ice cover suggests that there could be loss of Hg°_{diss} from the open waters within the ice. However, as there is no definitive answer in the literature, we have made gas exchange calculations assuming that there is little gas exchange in regions that are dominantly ice covered.

4.2. Hg° air-sea exchange

After using the atmospheric Hg° concentrations and calculated $k_{H'}$ values to calculate an equilibrium Hg°_{diss} concentration, we determined the percent saturation of Hg°_{diss} (Eq. (3)) in the surface waters of the Arctic (Fig. S6, Table 2). In the absence of contiguous sea ice, Hg°_{diss} concentrations were typically near saturation. On the western leg of the

Table 2
Summary of average Hg° concentrations in water ($[Hg^{\circ}_{diss}]$) and air ($[Hg^{\circ}_{atmos}]$) and average Hg° air-sea flux values in open water, the marginal ice zone (MIZ), and under contiguous ice. *Flux values under ice are theoretical, based on ice-free conditions.

	Open Water	MIZ	Contiguous Ice
$[Hg^{\circ}_{diss}]$ (fM)	32 ± 30	16 ± 17	101 ± 98
$[Hg^{\circ}_{atmos}]$ (ng m^{-3})	1.25 ± 0.10	1.24 ± 0.14	1.26 ± 0.08
% Saturation	97 ± 88	39 ± 46	230 ± 228
Hg Flux (pmol m^{-2} h^{-1})	2 ± 14	− 3 ± 5	14 ± 52*

cruise in open water (south of 73.5°N) the percent saturation was 61 ± 25%, while on the eastern return leg it was 145 ± 116%. The overall average percent saturation for open water was 97 ± 88%. Increased saturation on the eastern leg was a result of elevated Hg°_{diss} concentrations near shore. In the MIZ, where Hg°_{diss} concentrations had not had a chance to build (or rather had already evaded), the percent saturation was 39 ± 46%. Concentrations were strongly supersaturated under contiguous ice, increasing to an average of 230 ± 228% with a maximum of 1105%. The maximum degree of saturation observed by Andersson et al. (2008) in this region was 1800%. Undersaturation has sometimes been observed in other waters such as the South China Sea, where decreased production of Hg°_{diss} was attributed to low temperatures in the winter (Tseng et al., 2013). For many warmer regions of the ocean, such as the North Atlantic and Southeastern tropical Pacific, supersaturation has been observed, but not to the same extent that we calculated under the ice (e.g., Soerensen et al., 2014; Mason et al., 2017). Without the presence of sea ice, supersaturation is generally attributed to enhanced atmospheric deposition rates (high precipitation) and higher water temperatures; however, without sea ice acting as a barrier, these enhanced Hg°_{diss} levels simply lead to increased evasion before concentrations can rise to the levels we observed in the Arctic.

Estimated Hg°_{diss} evasion in the Arctic was largely minimal in open offshore waters (Fig. 7), with values similar in magnitude to fluxes estimated in other regions across the globe, from the Pacific and Atlantic Oceans to coastal waters (Andersson et al., 2007; Ci et al., 2016; Kuss et al., 2011; Mason et al., 1999; Soerensen et al., 2014). Toward the North Pole, there was the potential for higher evasion rates due to the elevated levels of Hg°_{diss}; however, the sea ice present acted as a barrier and prevents this flux from the ocean. A hypothetical flux was calculated regardless, using below ice water temperatures as well as local wind speed and Hg°_{atmos} concentrations. Open water Hg° fluxes averaged 2 ± 14 pmol m^{-2} h^{-1}, with an average of −2 ± 2 pmol m^{-2} h^{-1} on the western leg and 8 ± 19 pmol m^{-2} h^{-1} on the eastern return leg pmol m^{-2} h^{-1} of the cruise. In the MIZ, average fluxes were 3 ± 5 pmol m^{-2} h^{-1}, increasing to a potential flux (if the ice was removed) of 14 ± 52 pmol m^{-2} h^{-1} (Table 2) under contiguous ice. Maximum predicted evasion values reached 492 pmol m^{-2} h^{-1}, which was very similar to the maximum evasion rate observed by Andersson et al. (2008c) along the Alaskan coast (490 pmol m^{-2} h^{-1}). Kirk et al. (2008) calculated fluxes averaging 27 ± 29 pmol m^{-2} h^{-1} (ranging from 0.54 to 81 pmol m^{-2} h^{-1}) in the CAA and Hudson Bay between August and October, with higher fluxes predicted immediately following ice out.

As has been observed previously, variations in both Hg°_{diss} and wind speed drove the evasion of Hg° (Kuss et al., 2011; Soerensen et al., 2014, 2013). No significant change in air sea exchange was observed when moving off the continental shelf and approaching the MIZ. Because of the substantial differences between concentrations in ice-free and covered waters there were no general observable trends between the Hg°_{diss} concentrations and fluxes and other ancillary variables (Fig. S2). In addition to the elevated flux values during periods of elevated Hg°_{diss} levels, peaks in fluxes were also calculated at times of increased wind speed events because of the resulting increase in the mass transfer coefficient (Fig. S1), resulting in the spikes in fluxes observed in Fig. 7. Elevated evasion on the eastern leg of the cruise off the coast of Alaska was a result of higher Hg°_{diss} concentrations as well as increased winds.

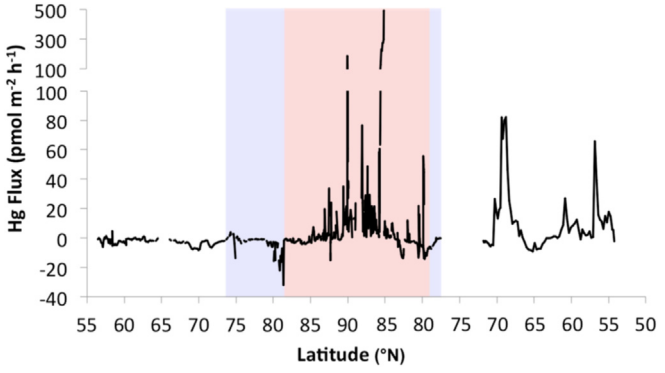

Fig. 7. Evasion of dissolved Hg° out of the surface ocean along the U.S. Arctic GEOTRACES cruise track. Values under ice cover (marginal ice: light blue, 73.5–81°N, 79–77.5°N; contiguous ice: pink 81–90–79°N) are theoretical fluxes. (For interpretation of the references to color in this figure legend, the reader is referred to the web version of this article).

The majority of the Hg°_{atmos} in the marine boundary layer is generally considered to have come from evasion from the surface ocean (Soerensen et al., 2010; Strode et al., 2007), so high Hg°_{diss} concentrations would ordinarily (in the absence of sea-ice) suggest the potential for elevated Hg°_{atmos} concentrations (Dastoor and Durnford, 2014). Despite increased Hg°_{diss} concentrations and percent saturation values over 100% at high latitudes, no significant increase in Hg°_{atmos} was observed as would be expected if this Hg°_{diss} was evading to the atmosphere. This observation supports our conclusion that sea ice acts as an effective barrier for the transport of volatile Hg°_{diss}. On the return leg of the cruise off the coast of Alaska (~ 70 – 55°N), where elevated Hg° fluxes were calculated in open water (Fig. 7), we did observe Hg°_{atmos} levels that were significantly higher ($p = 0.0003$) than the cruise average. Overall, average Hg°_{atmos} concentrations (1.25 ± 0.10 ng m^{-3}; Table 2) were generally lower than have been measured in coastal Arctic sites such as Alert, Canada, which averaged 1.49 ± 0.11 ng m^{-3} in the fall of 2002 (Kirk et al., 2012). This trend could have been a result of the proximity of these locations to Hg sources, or possibly changes in Hg° evasion due recent ice cover melting.

Accumulation of Hg°_{diss} under sea ice has obvious ramifications for Hg cycling in the future given the predicted changes in the timing and extent of annual ice coverage. Using the average surface concentration under the ice of 101 fM and a calculated average equilibrium concentration of 32 fM for the same region, along with an average k_w of 0.177 m h^{-1} based on measured wind speeds, we calculated the time to it would take for Hg° to establish equilibrium with the atmosphere after the theoretical sudden removal of sea ice from the contiguous ice zone. Flux rates were calculated hourly as surface concentrations dropped until equilibrium was reached. After 15.5 days the concentration was within 5% of the equilibrium value, and after 23 days it was within 1%. This timing makes sense based on previously observed peaks in atmospheric Hg° concentrations due to evasion from the surface ocean, which occur later than peaks due to revolatilization of Hg from snowmelt (Dastoor and Durnford, 2014). These calculations serve as a rough estimate, as the impact of other processes on the concentration of Hg° in the surface ocean (e.g., deposition and photochemical cycling) was neglected.

The timescale for the accumulation of Hg°_{diss} under the ice is more difficult to determine. Although a small portion of the UV radiation makes it through the ice (Perovich, 2006), net biological Hg(II) reduction is likely the primary pathway for Hg° formation in the Arctic compared to other oceans where photochemical reduction dominates (Kirk et al., 2012; Poulain et al., 2007; Soerensen et al., 2010). The unknown relative importance of dark (biological) and photochemical reduction and oxidation pathways make calculation of Hg°_{diss} accumulation time scales difficult. We expect Hg°_{diss} accumulation to the elevated levels observed to take days to weeks based on the our observation of low Hg°_{diss} concentrations in the MIZ, where water masses likely were not trapped under mobile ice sheets for very long. Rutgers van der Loeff et al. (2014) presented data showing a linear increase in ^{222}Rn with % ice cover, which we would expect for Hg°_{diss} if it was rapidly accumulated under the ice. Unlike Hg, the concentration of ^{222}Rn in the surface ocean is controlled by its formation from its radioactive parent ^{226}Ra ($t_{1/2}$ ≈ 1600 years), its decay ($t_{1/2}$ = 3.8 days)

and its evasion to the atmosphere, so ice cover results in a predictable change in surface water concentrations (Rutgers van der Loeff et al., 2014). Hg° air-sea exchange is complicated by the biological and photochemical pathways affecting its speciation. The low concentrations of Hg°_{diss} observed as ice cover began to increase in the MIZ (Fig. 6) indicate that these processes are slow to shift Hg speciation to its reduced form.

4.3. Precipitation and aerosols

Precipitation CH_3Hg and Hg_T concentrations were similar to those found in surface snow (Table 1). Hg_T concentrations were lower than reported in lower regions of the Arctic (e.g., Braune et al., 2015; Sanei et al., 2010). For example, annual mean Hg_T concentrations of 25–46 pM were reported in the Canadian sub-Arctic, with typical concentrations during the same period as this cruise falling in the lower end of this range (Sanei et al., 2010). Lower concentrations have been measured in open ocean regions of the central Pacific, averaging 11 ± 6 pM (Mason et al., 2017). CH_3Hg measurements in precipitation are more limited. While % CH_3Hg values were comparable to those found in other remote ocean locations, CH_3Hg concentrations in the North Atlantic averaged 0.41 ± 0.23 pM (Mason et al., 2017). Other studies in the Canadian Arctic Archipelago also found higher CH_3Hg concentrations averaging 0.13–0.50 pM (Hammerschmidt and Fitzgerald, 2006; Lehnherr et al., 2012).

In agreement with previous research (Cobbett et al., 2007; Kirk et al., 2006; Steffen et al., 2014), Hg_{PB} concentrations measured on aerosol filters (0.33 ± 0.34 pg m^{-3}) were low during the time of the cruise (following the spring AMDE). Cobbett et al., 2007 observed a peak in aerosol Hg concentrations in Alert, Canada during the transition between the polar night and polar day (February – March) as high as 693.9 pg m^{-3}, but concentrations dropped after this period due to decreasing aerosol concentrations. Minimum concentrations under 1 pg m^{-3} were reported in multiple studies for other periods of the year; they were generally lowest during August and September, the same time of year as the GN01 cruise (Cobbett et al., 2007; Steffen et al., 2014). Average concentrations were generally higher than measured during this study, possibly indicating a decreasing geographic trend in the presence of aerosols in the atmosphere.

The highest aerosol concentrations (Fig. S3) corresponded with the deployment that covered the region where there was a spike in Hg°_{diss} and drop in the concentration of Hg°_{atmos} at 75°N (Fig. S8), possibly indicating the scavenging of Hg°_{atmos} (due to oxidation to Hg_R) and deposition into the ocean. Holmes et al. (2009) suggested that any Hg_R produced in the marine boundary layer would be taken up by sea salt particles and rapidly removed from the atmosphere. However, our results do not clearly support such a mechanism, as there is no indication that the aerosol Hg is concentrated onto larger particulates.

Comparing aerosol Hg data to measurements of aluminum (Al; Marsay et al., 2018b), a crustal element that has little anthropogenic inputs to aerosols, we concluded that the aerosol Hg was not of crustal origin. The Hg/Al (g/g) ratios (Fig. S5) were well above the crustal ratio of $\sim 7 \times 10^{-8}$ (Mason et al., 2017). The lowest ratios were found near the pole and the highest closer to shore, indicating a larger influence of anthropogenic Hg near the continent.

4.4. Ice cores, surface snow and melt ponds

Hg concentrations in ice cores were generally low with higher concentrations at the surface, possibly due to scavenging of Hg_{PB} and Hg_R and the resulting atmospheric deposition, likely following spring AMDEs (Fisher et al., 2013; Steffen et al., 2014). Concentrations deeper in the core were lower, matching values found in surface waters under the ice (0.1 ± 0.1 pM CH_3Hg, 1.4 ± 0.4 pM Hg_T; Bowman, Agather, 2018). Because samples were unfiltered, higher values of % CH_3Hg found could indicate either patches of biogenic particles (algae), or possibly regions of methylation in the ice (Gionfriddo et al., 2016). Average Hg_T and CH_3Hg concentrations (2.8 and 0.086 pM, respectively; Table 1) were very similar to other studies in the Arctic and Antarctic (Beattie et al., 2014; Chaulk et al., 2011; Cossa et al., 2011).

In first year ice in the Southern Beaufort Sea of the Arctic, Chaulk et al. (2011) found low and consistent concentrations measuring ~2.5 pM in most of the core, with higher values up to 15 pM at the ice-snow interface. In multi-year ice, concentrations above 20 pM were found at the surface. The Hg_T concentrations again decreased sharply with depth, but unique to the multi-year ice were cyclic features with several peaks rising to ~8 pM. Similar to our study, concentrations deeper in the core were comparable to the underlying water. Other measurements of Hg concentrations in multi-year ice in the Beaufort Sea and McClure Strait were made by Beattie et al. (2014). Trends with depth were similar, but concentrations rose moving from the Beaufort Sea into the McClure Strait, with Hg_T concentrations reaching as high as 60.8 pM in surface ice. CH_3Hg averaged 0.20 pM in the Beaufort Sea ice, but rose to 1.35 pM in the McClure Strait. Percent CH_3Hg ranged from 2.3% to 40.9%, peaking in the mid to bottom sections of the ice, possibly suggesting in situ methylation. In the Southern Ocean, Cossa et al. (2011) also measured higher Hg_T concentrations at the surface of ice cores, with average concentrations deeper in the core around 3 pM. CH_3Hg concentrations were relatively consistent throughout the core, with concentrations up to almost 0.4 pM. Clearly, while there is the possibility of higher concentrations in coastal ice regions based on the collections in both the Arctic and Antarctic discussed above, our data do not suggest that these high concentrations persist in ice collected further offshore. These differences suggest that data from ice cores in the coastal Arctic should not be extrapolated to the central basin as these data are not likely representative of the Arctic open waters.

Previous measurements in surface snow have focused on periods following AMDEs given the dramatic changes that can occur due to deposition of oxidized Hg, resulting in concentrations that are much higher than those measured here. Studies indicate that a significant portion of the Hg deposited is quickly reduced and emitted back to the atmosphere (Kirk et al., 2012, 2006; Steffen et al., 2015), potentially increasing Hg°_{atmos} concentrations in conjunction with greater Hg°_{diss} evasion following sea ice melt (Angot et al., 2016). St Louis et al. (2007), for example, measured decreasing concentrations in the snowpack in Alert into June, with Hg_T concentrations dropping below 5 pM later in the season. CH_3Hg concentrations also fell below 1 pM, especially in the base of the snowpack. Percent CH_3Hg was low at the surface (0.4 ± 0.5%), but increased in the depth hoar snow (3.6 ± 7.0%). On the Hudson Bay, Kirk et al. (2006) measured concentrations of Hg_T in surface snow as high as 3.30 nM in the spring of 2003, but concentrations dropped to ~25 pM within days. Lu et al. (2001) measured Hg_T in sea ice snow in the Beaufort Sea, finding concentrations as low as ~13 pM between November and December, with concentrations rising throughout the spring. Chaulk et al. (2011) measured Hg_T concentrations less than 5 pM in snow from the coastal Beaufort Sea, with higher peaks due to atmospheric deposition. Our Hg_T concentrations (3.6 ± 1.3 pM) indicate that Hg levels in surface snow in the Central Basin in the late summer and fall were even lower than many coastal locations. These concentrations are valuable in understanding the importance of surface snow and ice as a source of Hg to the biosphere. The low concentrations observed could be indicative of low levels of Hg in late summer snow, or possibly the evasion of the Hg that may have accumulated over springtime AMDEs. Melting snowpack releases water soluble oxidized Hg(II) to the surface ocean, while Hg° can be volatilized back to the atmosphere following the reduction of Hg(II) (Chaulk et al., 2011; Lu et al., 2001).

Concentrations of CH_3Hg in melt ponds (97 ± 75 fM) were similar to that of ice, but were significantly higher ($p = 0.0023$) than concentrations found in surface snow. Total Hg in melt ponds was significantly higher ($p < 0.05$) than in both ice cores and surface snow, largely because of higher concentrations found at station 46. These data

therefore provide some evidence for Hg accumulation in melt ponds, in contrast to data presented by Aspmo et al. (2006) form the North Atlantic showing no long-term accumulation. Based on other trace element concentrations (Marsay et al., 2018a), it is clear that these melt ponds represented a transitional environment with influences from processes such as seawater intrusion, photochemical redox cycling, and atmospheric deposition. Future changes in sea ice dynamics may therefore impact the release and ensuing accumulation of Hg contained in snow, ice, and melt ponds into the aquatic food web.

4.5. Mass balance

Due to temporal variability during the times of the year not covered by the cruise, especially given the potentially high exchange during polar sunrise where AMDEs and Hg deposition are heightened, estimates of wet and dry deposition were calculated on a monthly basis to represent values during the time of the cruise. The overall low precipitation (340 mm yr^{-1}; Serreze et al., 2006) at high latitudes results in relatively low wet deposition of Hg to the Arctic. Monthly wet deposition, calculated using the measured concentrations, Arctic Ocean surface area and yearly precipitation, was estimated to be 7.6 mol of CH_3Hg and 1.0 kmol of Hg_T. Based on the measurements in aerosols and an estimated dry deposition velocity of 0.5 cm s^{-1} (Holmes et al., 2009), given that there appeared to be mainly fine particulate aerosols, 1.0 mol of CH_3Hg and 0.24 kmol of Hg_T were deposited per month via dry aerosol deposition. Similarly, Hg_R was deposited at a rate of 1.5 kmol mth^{-1}. The total atmospheric deposition to the surface Arctic Ocean was thus estimated as 8.6 mol mth^{-1} CH_3Hg and 2.7 kmol mth^{-1} Hg_T. Wet deposition represented 88% of the CH_3Hg flux and 38% of the Hg_T flux, with dry deposition making up the remainder. In other parts of the world, greater precipitation typically results in a greater importance of wet deposition to the Hg_T flux (e.g., Gichuki and Mason, 2014). These calculations also did not include reactive gaseous CH_3Hg (CH_3Hg_R), which was not measured, but previous studies have shown that it might constitute up to 25% of Hg_R (Baya et al., 2015). Even at a much lower percentage, CH_3Hg_R could dominate dry CH_3Hg deposition and thus decrease the importance of wet deposition. Atmospheric inputs of CH_3Hg and Hg_T were estimated to be much higher by Soerensen et al. (2016), with average monthly fluxes of 3.3 kmol mth^{-1} CH_3Hg and 12.5 kmol mth^{-1} Hg_T. Their estimate of CH_3Hg atmospheric deposition was much greater possibly in part due to the inclusion of CH_3Hg produced by the degradation of dimethylmercury ($(CH_3)_2Hg$) in the atmosphere. However, recent measurements of $(CH_3)_2Hg$ in Arctic surface waters from this and other cruises suggest that evasional fluxes of $(CH_3)_2Hg$ from the surface ocean may have been overestimated in the Soerensen et al. model (A. Agather and S. Jonsson, personal comm.). In addition, our measurements were made outside of the spring AMDE period when deposition is typically much greater (e.g., Steffen et al., 2008), which was included in the average monthly flux reported above from Soerensen et al. (2016).

For gas exchange, applying the overall average calculated Hg^0 evasion rate to the entire Arctic (8.2 pmol m^{-2} h^{-1}) is unreasonable because evasion does not occur under ice where predicted fluxes are greatest. Applying the average Hg^0 flux in open waters (2.1 pmol m^{-2} h^{-1}) to the average area of open water (40.3% open water; 11.1×10^6 km^2 total area with 6.65×10^6 km^2 ice coverage; National Snow and Ice Data Center (NSIDC), 2016; Soerensen et al., 2016), we calculated an evasion of 6.8 kmol mth^{-1}. This flux, calculated for the fall period in which the GN01 cruise took place, is about five times lower than the average monthly flux reported by Soerensen et al. (2016) (35 kmol mth^{-1}). As we cannot account for the evasion of Hg deposited on snow and ice cover or the input of Hg from snow and ice melt, it is difficult to directly quantify a net flux of Hg to the central Arctic using our data. Soerensen et al. (2016) estimated that atmospheric deposition and snow and ice melt inputs were similar in magnitude, which would bring our estimated inputs of Hg closer to the evasion flux. Coastal and riverine inputs and/or water transport from the Atlantic and Pacific, along with increased deposition at other times of the year, could ultimately result in sources of Hg to the Arctic outweighing the sinks.

5. Conclusions

Dissolved and atmospheric Hg^0 concentrations, measured continuously at high temporal resolution in Arctic Ocean during late summer and early fall, have further contributed to our understanding of the air-sea exchange of Hg in the Arctic. Our data suggest that sea ice plays a large role in the accumulation of Hg^0_{diss} in the surface Arctic Ocean. While concentrations averaged 32 ± 30 fM in open water, they rose as high as 544 fM under contiguous ice. This increase confirms the previous observations of the accumulation of Hg^0_{diss} in the Arctic during periods of ice coverage. This trend was attributed to sea ice acting as a barrier for Hg^0 air-sea exchange and the continued net formation of Hg^0, even under the ice in the absence of elevated radiation levels. Because variations in atmospheric Hg^0 concentrations (averaging 1.2 ± 0.1 ng m^{-3}) were relatively small, wind speed and Hg^0_{diss} concentrations were the major drivers of the predicted Hg^0 evasional flux.

Measurements of CH_3Hg and Hg_T in precipitation and aerosols in the central Arctic also substantially added to our previous knowledge, as much of the previous research has focused on measurements made from or near land. Our results suggest that aerosol concentrations and deposition rates in the open waters of the Arctic are much lower than in coastal regions and the Canadian Arctic Archipelago during this time period. Levels of Hg in fine and bulk aerosols were similar, suggesting that the uptake of Hg_R into aerosols was not an important mechanism for Hg_R removal during the time of the cruise.

Ice core and surface snow measurements also helped quantify the amount of Hg that could be entering the ocean through ice melt in the central Arctic. Initially, melting sea ice in a warming climate will likely lead to increased Hg^0 evasion, resulting in decreased Hg levels in the surface Arctic Ocean. Subsaturated concentrations in other parts of the Arctic however suggest an eventual decrease in evasion in the absence of sea ice. These additional insights and high resolution measurements will help to further refine global and regional Hg models, improving their ability to predict future changes in Hg transport and transformations within diverse marine ecosystems. Future studies focusing on air-sea exchange dynamics in marginal ice zones will also aid in understanding the extent of Hg^0 evasion in open leads and polynyas in the Arctic.

Acknowledgements

We would like to thank the captain and crew of the ship, the USCGC *Healy*, as well as our colleagues on the U.S. Arctic GEOTRACES cruise, especially: Cliff Buck, Pete Morton, and Brent Summers for collection of the atmospheric samples; Ana Aguilar-Islas, Rob Rember, and Bill Landing for ice core, snow, and melt pond sampling; and Carl Lamborg, Katlin Bowman, and Alison Agather for sample preparation and storage. We would also like to thank Prentiss Balcom for pre-cruise preparation including the underway sampling equipment. This study was funded by the National Science Foundation (NSF) Chemical Oceanography Program through grant #1434998, and was part of the Ph.D. thesis of Brian DiMento.

Appendix A. Supporting information

Supplementary data associated with this article can be found in the online version at doi:10.1016/j.dsr.2018.12.001.

References

Agather A.M., 2018. Geochemical and microbiological controls on mercury methylation in natural waters. PhD Thesis, Wright State University.

AMAP, 2011. AMAP Assessment 2011: mercury in the Arctic. Arctic Monitoring and Assessment Programme, Oslo, Norway.
Amyot, M., Gill, G.A., Morel, F.M.M., 1997. Production and loss of dissolved gaseous mercury in coastal seawater. Environ. Sci. Technol. 31, 3606–3611. https://doi.org/10.1021/es9703685.
Amyot, M., McQueen, D.J., Mierle, G., Lean, D.R.S., 1994. Sunlight-induced formation of dissolved gaseous mercury in lake waters. Environ. Sci. Technol. 28, 2366–2371. https://doi.org/10.1021/es00062a022.
Andersson, M.E., Gårdfeldt, K., Wängberg, I., 2008a. A description of an automatic continuous equilibrium system for the measurement of dissolved gaseous mercury. Anal. Bioanal. Chem. 391, 2277–2282. https://doi.org/10.1007/s00216-008-2127-4.
Andersson, M.E., Gårdfeldt, K., Wängberg, I., Sprovieri, F., Pirrone, N., Lindqvist, O., 2007. Seasonal and daily variation of mercury evasion at coastal and off shore sites from the Mediterranean Sea. Mar. Chem. 104, 214–226. https://doi.org/10.1016/j.marchem.2006.11.003.
Andersson, M.E., Gårdfeldt, K., Wängberg, I., Strömberg, D., 2008b. Determination of Henry's law constant for elemental mercury. Chemosphere 73, 587–592. https://doi.org/10.1016/j.chemosphere.2008.05.067.
Andersson, M.E., Sommar, J., Gårdfeldt, K., Lindqvist, O., 2008c. Enhanced concentrations of dissolved gaseous mercury in the surface waters of the Arctic Ocean. Mar. Chem. 110, 190–194. https://doi.org/10.1016/j.marchem.2008.04.002.
Angot, H., Dastoor, A., De Simone, F., Gårdfeldt, K., Gencarelli, C.N., Hedgecock, I.M., Langer, S., Magand, O., Mastromonaco, M.N., Nordstrøm, C., Pfaffhuber, K.A., Pirrone, N., Ryjkov, A., Selin, N.E., Skov, H., Song, S., Sprovieri, F., Steffen, A., Toyota, K., Travnikov, O., Yang, X., Dommergue, A., 2016. Chemical cycling and deposition of atmospheric mercury in polar regions: review of recent measurements and comparison with models. Atmos. Chem. Phys. 16, 10735–10763. https://doi.org/10.5194/acp-16-10735-2016.
Ariya, P.A., Dastoor, A.P., Amyot, M., Schroeder, W.H., Barrie, L., Anlauf, K., Raofie, F., Ryzhkov, A., Davignon, D., Lalonde, J., Steffen, A., 2004. The Arctic: a sink for mercury. Tellus B 56, 397–403. https://doi.org/10.1111/j.1600-0889.2004.00118.x.
Aspmo, K., Temme, C., Berg, T., Ferrari, C., Gauchard, P.-A., Fain, X., Wibetoe, G., 2006. Mercury in the atmosphere, snow and melt water ponds in the North Atlantic Ocean during Arctic Summer. Environ. Sci. Technol. 40, 4083–4089. https://doi.org/10.1021/es052117z.
Bais, A.F., Tourpali, K., Kazantzidis, A., Akiyoshi, H., Bekki, S., Braesicke, P., Chipperfield, M.P., Dameris, M., Eyring, V., Garny, H., Iachetti, D., Jöckel, P., Kubin, A., Langematz, U., Mancini, E., Michou, M., Morgenstern, O., Nakamura, T., Newman, P.A., Pitari, G., Plummer, D.A., Rozanov, E., Shepherd, T.G., Shibata, K., Tian, W., Yamashita, Y., 2011. Projections of UV radiation changes in the 21st century: impact of ozone recovery and cloud effects. Atmos. Chem. Phys. 11, 7533–7545. https://doi.org/10.5194/acp-11-7533-2011.
Baya, P.A., Gosselin, M., Lehnherr, I., St Louis, V.L., Hintelmann, H., 2015. Determination of monomethylmercury and dimethylmercury in the arctic marine boundary layer. Environ. Sci. Technol. 49, 223–232. https://doi.org/10.1021/es502601z.
Beattie, S.A., Armstrong, D., Chaulk, A., Comte, J., Gosselin, M., Wang, F., 2014. Total and methylated mercury in arctic multiyear sea ice. Environ. Sci. Technol. 48, 5575–5582. https://doi.org/10.1021/es5008033.
Bekryaev, R.V., Polyakov, I.V., Alexeev, V.A., 2010. Role of polar amplification in long-term surface air temperature variations and modern arctic warming. J. Clim. 23, 3888–3906. https://doi.org/10.1175/2010JCLI3297.1.
Bintanja, R., Graversen, R.G., Hazeleger, W., 2011. Arctic winter warming amplified by the thermal inversion and consequent low infrared cooling to space. Nat. Geosci. 4, 758–761. https://doi.org/10.1038/ngeo1285.
Braune, B., Chételat, J., Amyot, M., Brown, T., Clayden, M., Evans, M., Fisk, A., Gaden, A., Girard, C., Hare, A., Kirk, J., Lehnherr, I., Letcher, R., Loseto, L., Macdonald, R., Mann, E., McMeans, B., Muir, D., O'Driscoll, N., Poulain, A., Reimer, K., Stern, G., 2015. Mercury in the marine environment of the Canadian Arctic: review of recent findings. Sci. Total Environ. 509–510, 67–90. https://doi.org/10.1016/j.scitotenv.2014.05.133.
Brunke, E.-G., Labuschagne, C., Ebinghaus, R., Kock, H.H., Slemr, F., 2010. Gaseous elemental mercury depletion events observed at Cape Point during 2007–2008. Atmos. Chem. Phys. 10, 1121–1131. https://doi.org/10.5194/acp-10-1121-2010.
Cavalieri, D.J., Parkinson, C.L., 2012. Arctic sea ice variability and trends, 1979–2010. Cryosphere 6, 881–889. https://doi.org/10.5194/tc-6-881-2012.
Chaulk, A., Stern, G.A., Armstrong, D., Barber, D.G., Wang, F., 2011. Mercury distribution and transport across the ocean – sea-ice – atmosphere interface in the Arctic Ocean. Environ. Sci. Technol. 45, 1866–1872. https://doi.org/10.1021/es103434c.
Ci, Z., Zhang, X., Wang, Z., 2016. Air–sea exchange of gaseous mercury in the tropical coast (Luhuitou fringing reef) of the South China Sea, the Hainan Island, China. Environ. Sci. Pollut. Res. 1–7. https://doi.org/10.1007/s11356-016-6346-5.
Clarkson, T.W., Magos, L., 2006. The toxicology of mercury and its chemical compounds. Crit. Rev. Toxicol. 36, 609–662. https://doi.org/10.1080/10408440600845619.
Cobbett, F.D., Steffen, A., Lawson, G., Van Heyst, B.J., 2007. GEM fluxes and atmospheric mercury concentrations (GEM, RGM and Hgp) in the Canadian Arctic at Alert, Nunavut, Canada (February–June 2005). Atmos. Environ. 41, 6527–6543. https://doi.org/10.1016/j.atmosenv.2007.04.033.
Corbitt, E.S., Jacob, D.J., Holmes, C.D., Streets, D.G., Sunderland, E.M., 2011. Global source-receptor relationships for mercury deposition under present-day and 2050 emissions scenarios. Environ. Sci. Technol. 45, 10477–10484.
Cossa, D., Heimbürger, L.E., Lannuzel, D., Rintoul, S.R., Butler, E.C.V., Bowie, A.R., Averty, B., Watson, R.J., Remenyi, T., 2011. Mercury in the southern ocean. Geochim. Cosmochim. Acta 75, 4037–4052. https://doi.org/10.1016/j.gca.2011.05.001.
Dastoor, A., Ryzhkov, A., Durnford, D., Lehnherr, I., Steffen, A., Morrison, H., 2015. Atmospheric mercury in the Canadian Arctic. Part II: insight from modeling. Sci. Total Environ. 509–510, 16–27. https://doi.org/10.1016/j.scitotenv.2014.10.112.
Dastoor, A.P., Durnford, D.A., 2014. Arctic Ocean: is it a sink or a source of atmospheric mercury? Environ. Sci. Technol. 48, 1707–1717. https://doi.org/10.1021/es404473e.
Driscoll, C.T., Mason, R.P., Chan, H.M., Jacob, D.J., Pirrone, N., 2013. Mercury as a global pollutant: sources, pathways, and effects. Environ. Sci. Technol. 47, 4967–4983. https://doi.org/10.1021/es305071v.
Fanning, K.A., Torres, L.M., 1991. ^{222}Rn and ^{226}Ra: indicators of sea-ice effects on air-sea gas exchange. Polar Res. 10, 51–58. https://doi.org/10.1111/j.1751-8369.1991.tb00634.x.
Fisher, J.A., Jacob, D.J., Soerensen, A.L., Amos, H.M., Steffen, A., Sunderland, E.M., 2012. Riverine source of Arctic Ocean mercury inferred from atmospheric observations. Nat. Geosci. 5, 499–504. https://doi.org/10.1038/ngeo1478.
Fisher, J.A., Jacob, D.J., Soerensen, A.L., Amos, H.M., Corbitt, E.S., Streets, D.G., Wang, Q., Yantosca, R.M., Sunderland, E.M., 2013. Factors driving mercury variability in the Arctic atmosphere and ocean over the past 30 years. Glob. Biogeochem. Cycles 27, 1226–1235. https://doi.org/10.1002/2013GB004689.
Fitzgerald, W.F., Lamborg, C.H., Hammerschmidt, C.R., 2007. Marine biogeochemical cycling of mercury. Chem. Rev. 107, 641–662. https://doi.org/10.1021/cr050353m.
Gichuki, S.W., Mason, R.P., 2014. Wet and dry deposition of mercury in Bermuda. Atmos. Environ. 87, 249–257. https://doi.org/10.1016/j.atmosenv.2014.01.025.
Gionfriddo, C.M., Tate, M.T., Wick, R.R., Schultz, M.B., Zemla, A., Thelen, M.P., Schofield, R., Krabbenhoft, D.P., Holt, K.E., Moreau, J.W., 2016. Microbial mercury methylation in Antarctic sea ice. Nat. Microbiol. 1–12. https://doi.org/10.1038/nmicrobiol.2016.127.
Hammerschmidt, C.R., Fitzgerald, W.F., 2005. Methylmercury in mosquitoes related to atmospheric mercury deposition and contamination. Environ. Sci. Technol. 39, 3034–3039. https://doi.org/10.1021/es0485107.
Hammerschmidt, C.R., Fitzgerald, W.F., 2006. Bioaccumulation and trophic transfer of methylmercury in Long Island Sound. Arch. Environ. Contam. Toxicol. 51, 416–424. https://doi.org/10.1007/s00244-005-0265-7.
Heimbürger, L.-E., Sonke, J.E., Cossa, D., Point, D., Lagane, C., Laffont, L., Galfond, B.T., Nicolaus, M., Rabe, B., van der Loeff, M.R., 2015. Shallow methylmercury production in the marginal sea ice zone of the central Arctic Ocean. Nat. Publ. Group 1–6. https://doi.org/10.1038/srep10318.
Holmes, C.D., Jacob, D.J., Mason, R.P., Jaffe, D.A., 2009. Sources and deposition of reactive gaseous mercury in the marine atmosphere. Atmos. Environ. 43, 2278–2285. https://doi.org/10.1016/j.atmosenv.2009.01.051.
Kim, H., Rhee, T.S., Hahm, D., Hwang, C.Y., Yang, J., Han, S., 2016. Contrasting distributions of dissolved gaseous mercury concentration and evasion in the North Pacific Subarctic Gyre and the Subarctic Front. Deep-Sea Res. Part I 110, 90–98. https://doi.org/10.1016/j.dsr.2016.02.001.
Kirk, J.L., Lehnherr, I., Andersson, M., Braune, B.M., Chan, L., Dastoor, A.P., Durnford, D., Gleason, A.L., Loseto, L.L., Steffen, A., St Louis, V.L., 2012. Mercury in Arctic marine ecosystems: sources, pathways and exposure. Environ. Res. 119, 64–87. https://doi.org/10.1016/j.envres.2012.08.012.
Kirk, J.L., Louis, V.S., Sharp, M.J., 2006. Rapid reduction and reemission of mercury deposited into snowpacks during atmospheric mercury depletion events at Churchill, Manitoba, Canada. Environ. Sci. Technol. 40, 7590–7596. https://doi.org/10.1021/es061299.
Kirk, J.L., St. Louis, V.L., Hintelmann, H., Lehnherr, I., Else, B., Poissant, L., 2008. Methylated mercury species in marine waters of the Canadian High and Sub Arctic. Environ. Sci. Technol. 42, 8367–8373. https://doi.org/10.1021/es801635m.
Kuss, J., Zülicke, C., Pohl, C., Schneider, B., 2011. Atlantic mercury emission determined from continuous analysis of the elemental mercury sea-air concentration difference within transects between 50°N and 50°S. Glob. Biogeochem. Cycles 25. https://doi.org/10.1029/2010GB003998.
Lalonde, J.D., Poulain, A.J., Amyot, M., 2002. The role of mercury redox reactions in snow on snow-to-air mercury transfer. Environ. Sci. Technol. 36, 174–178. https://doi.org/10.1021/es010786g.
Lamborg, C.H., Bowman, K., Hammerschmidt, C.R., Gilmour, C., Munson, K., Selin, N., Tseng, C.-M., 2014. Mercury in the Anthropocene Ocean. Oceanography 27, 76–87. https://doi.org/10.5670/oceanog.2014.11.
Lamborg, C.H., Hammerschmidt, C.R., Gill, G.A., Mason, R.P., Gichuki, S., 2012. An intercomparison of procedures for the determination of total mercury in seawater and recommendations regarding mercury speciation during GEOTRACES cruises. Limnol. Oceanogr. Methods 10, 90–100. https://doi.org/10.4319/lom.2012.10.90.
Landis, M.S., Stevens, R.K., Schaedlich, F., Prestbo, E.M., 2002. Development and characterization of an annular denuder methodology for the measurement of divalent inorganic reactive gaseous mercury in ambient air. Environ. Sci. Technol. 36, 3000–3009. https://doi.org/10.1021/es015887t.
Laurier, F., Mason, R.P., Whalin, L., Kato, S., 2003. Reactive gaseous mercury formation in the North Pacific Ocean's marine boundary layer: a potential role of halogen chemistry. J. Geophys. Res. 108. https://doi.org/10.1029/2003JD003625.
Lehnherr, I., St. Louis, V.L., Emmerton, C.A., Barker, J.D., Kirk, J.L., 2012. Methylmercury cycling in High Arctic wetland ponds: sources and sinks. Environ. Sci. Technol. 46, 10514–10522.
Lindberg, S., Bullock, R., Ebinghaus, R., Engstrom, D., Feng, X., Fitzgerald, W., Pirrone, N., Prestbo, E., Seigneur, C., Panel on Source Attribution of Atmospheric Mercury, 2007. A synthesis of progress and uncertainties in attributing the sources of mercury in deposition. Ambio 36, 19–32.
Lindberg, S.E., Brooks, S., Lin, C.J., Scott, K., Meyers, T., Chambers, L., Landis, M., Stevens, R., 2001. Formation of reactive gaseous mercury in the Arctic: evidence of oxidation of Hg° to gas- phase Hg-II compounds. Water Air, Soil Pollut.: Focus 1, 295–302. https://doi.org/10.1023/A:1013171509022.
Loose, B., McGillis, W.R., Schlosser, P., Perovich, D., Takahashi, T., 2009. Effects of

freezing, growth, and ice cover on gas transport processes in laboratory seawater experiments. Geophys. Res. Lett. 36, L05603. https://doi.org/10.1029/2008GL036318.
Loose, B., Miller, L.A., Elliott, S., Papakyriakou, T., 2011. Sea ice biogeochemistry and material transport across the frozen interface. Oceanography 24, 202–218.
Lu, J.Y., Schroeder, W.H., Barrie, L.A., Steffen, A., Welch, H.E., Martin, K., Lockhart, L., Hunt, R.V., Boila, G., Richter, A., 2001. Magnification of atmospheric mercury deposition to polar regions in springtime: the link to tropospheric ozone depletion chemistry. Geosphys. Res. Lett. 28, 3219–3222. https://doi.org/10.1029/2000GL012603.
Macdonald, R.W., Harner, T., Fyfe, J., 2005. Recent climate change in the Arctic and its impact on contaminant pathways and interpretation of temporal trend data. Sci. Total Environ. 342, 5–86. https://doi.org/10.1016/j.scitotenv.2004.12.059.
Mahaffey, K.R., Sunderland, E.M., Chan, H.M., Choi, A.L., Grandjean, P., Mariën, K., Oken, E., Sakamoto, M., Schoeny, R., Weihe, P., Yan, C.-H., Yasutake, A., 2011. Balancing the benefits of n-3 polyunsaturated fatty acids and the risks of methylmercury exposure from fish consumption. Nutr. Rev. 69, 493–508. https://doi.org/10.1111/j.1753-4887.2011.00415.x.
Marsay, C.M., Aguilar-Islas, A., Fitzsimmons, J.N., Hatta, M., Jensen, L.T., John, S.G., Kadko, D., Landing, W.M., Lanning, N.T., Morton, P.L., Pasqualini, A., Rauschenberg, S., Sherrell, R.M., Shiller, A.M., Twining, B.S., Whitmore, L.M., Zhang, R., Buck, C.S., 2018a. Dissolved and particulate trace elements in late summer Arctic melt ponds. Mar. Chem. 204, 70–85. https://doi.org/10.1016/j.marchem.2018.06.002.
Marsay, C.M., Kadko, D., Landing, W.M., Morton, P.L., Summers, B.A., Buck, C.S., 2018b. Concentrations, provenance and flux of aerosol trace elements during US GEOTRACES Western Arctic cruise GN01. Chem. Geol. 1–14. https://doi.org/10.1016/j.chemgeo.2018.06.007.
Mason, R.P., Choi, A.L., Fitzgerald, W.F., Hammerschmidt, C.R., Lamborg, C.H., Soerensen, A.L., Sunderland, E.M., 2012. Mercury biogeochemical cycling in the ocean and policy implications. Environ. Res. 119, 101–117. https://doi.org/10.1016/j.envres.2012.03.013.
Mason, R.P., Hammerschmidt, C.R., Lamborg, C.H., Bowman, K.L., Swarr, G.J., Shelley, R.U., 2017. The air-sea exchange of mercury in the low latitude Pacific and Atlantic Oceans. Deep Sea Res. Part I 122, 17–28. https://doi.org/10.1016/j.dsr.2017.01.015.
Mason, R.P., Lawson, N.M., Lawrence, A.L., Leaner, J.J., Lee, J.G., Sheu, G.-R., 1999. Mercury in the Chesapeake Bay. Mar. Chem. 65, 77–96. https://doi.org/10.1016/S0304-4203(99)00012-2.
Mason, R.P., Rolfhus, K.R., Fitzgerald, W.F., 1998. Mercury in the North Atlantic. Mar. Chem. 61, 37–53. https://doi.org/10.1016/S0304-4203(98)00006-1.
Morton, P.L., Landing, W.M., Hsu, S.-C., Milne, A., Aguilar-Islas, A.M., Baker, A.R., Bowie, A.R., Buck, C.S., Gao, Y., Gichuki, S., Hastings, M.G., Hatta, M., Johansen, A.M., Losno, R., Mead, C., Patey, M.D., Swarr, G., Vandermark, A., Zamora, L.M., 2013. Methods for the sampling and analysis of marine aerosols: results from the 2008 GEOTRACES aerosol intercalibration experiment. Limnol. Ocean. Methods 11, 62–78. https://doi.org/10.4319/lom.2013.11.62.
Munson, K.M., Babi, D., Lamborg, C.H., 2014. Determination of monomethylmercury from seawater with ascorbic acid-assisted direct ethylation. Limnol. Ocean. Methods 12, 1–9. https://doi.org/10.4319/lom.2014.12.1.
National Snow and Ice Data Center (NSIDC), 2016. Antarctic Sea Ice Extent [WWW Document]. httpnsidc.orgarcticseaicenewscharctic-interactive-sea-ice-graph. URL (Accessed 24 December 2016).
Nerentorp Mastromonaco, M.G., Gårdfeldt, K., Assmann, K.M., Langer, S., Delali, T., Shlyapnikov, Y.M., Zivkovic, I., Horvat, M., 2017a. Speciation of mercury in the waters of the Weddell, Amundsen and Ross Seas (Southern Ocean). Mar. Chem. 193, 20–33. https://doi.org/10.1016/j.marchem.2017.03.001.
Nerentorp Mastromonaco, M., Gårdfeldt, K., Jourdain, B., Abrahamsson, K., Granfors, A., Ahnoff, M., Dommergue, A., Méjean, G., Jacobi, H.W., 2016. Antarctic winter mercury and ozone depletion events over sea ice. Atmos. Environ. 129, 125–132. https://doi.org/10.1016/j.atmosenv.2016.01.023.
Nerentorp Mastromonaco, M.G., Gårdfeldt, K., Langer, S., 2017b. Mercury flux over West Antarctic Seas during winter, spring and summer. Mar. Chem. 193, 44–54. https://doi.org/10.1016/j.marchem.2016.08.005.
NOAA Climate.gov, 2016. [NOAAClimate], December 13). Arctic sea ice growing younger, thinner. Retrieved from ⟨https://www.youtube.com/watch?V=c6jX9URzZWg⟩.
O'Driscoll, N.J., Siciliano, S.D., Lean, D.R.S., Amyot, M., 2006. Gross photoreduction kinetics of mercury in temperate freshwater lakes and rivers: application to a general model of DGM dynamics. Environ. Sci. Technol. 40, 837–843. https://doi.org/10.1021/es051062y.
Outridge, P.M., Macdonald, R.W., Wang, F., Stern, G.A., Dastoor, A.P., 2008. A mass balance inventory of mercury in the Arctic Ocean. Environ. Chem. 5https://doi.org/10.1071/EN08002. (89–23).
Parkinson, C.L., Cavalieri, D.J., 2008. Arctic sea ice variability and trends, 1979–2006. J. Geophys. Res. 113, C07003–C07028. https://doi.org/10.1029/2007JC004558.
Perovich, D.K., 2006. The interaction of ultraviolet light with Arctic sea ice during SHEBA. Ann. Glaciol.
Poulain, A.J., Ni Chadhain, S.M., Ariya, P.A., Amyot, M., Garcia, E., Campbell, P.G.C., Zylstra, G.J., Barkay, T., 2007. Potential for mercury reduction by microbes in the high arctic. Appl. Environ. Microbiol. 73, 2230–2238. https://doi.org/10.1128/AEM.02701-06.
Rutgers van der Loeff, M.M., Cassar, N., Nicolaus, M., Rabe, B., Stimac, I., 2014. The influence of sea ice cover on air-sea gas exchange estimated with radon-222 profiles. J. Geophys. Res. -Oceans 119, 2735–2751. https://doi.org/10.1002/2013JC009321.
Sanei, H., Outridge, P.M., Goodarzi, F., Wang, F., Armstrong, D., Warren, K., Fishback, L., 2010. Wet deposition mercury fluxes in the Canadian sub-Arctic and southern Alberta, measured using an automated precipitation collector adapted to cold regions. Atmos. Environ. 44, 1672–1681. https://doi.org/10.1016/j.atmosenv.2010.01.030.
Schlitzer, R., 2015. Ocean Data View, odv.awi.de.
Schroeder, W.H., Anlauf, K.G., Barrie, L.A., Lu, J.Y., Steffen, A., Schneeberger, D.R., Berg, T., 1998. Arctic springtime depletion of mercury. Nature 394, 331–332. https://doi.org/10.1038/28530.
Screen, J.A., Simmonds, I., 2010. The central role of diminishing sea ice in recent Arctic temperature amplification. Nature 464, 1334–1337. https://doi.org/10.1038/nature09051.
Serreze, M.C., Barrett, A.P., Slater, A.G., Woodgate, R.A., Aagaard, K., Lammers, R.B., Steele, M., Moritz, R., Meredith, M., Lee, C.M., 2006. The large-scale freshwater cycle of the Arctic. J. Geophys. Res. 111https://doi.org/10.1029/2005JC003424. (14485–20).
Slemr, F., Schuster, G., Seiler, W., 1985. Distribution, speciation, and budget of atmospheric mercury. J. Atmos. Chem. 3, 407–434. https://doi.org/10.1007/BF00053870.
Soerensen, A.L., Jacob, D.J., Schartup, A., 2016. A mass budget for mercury and methylmercury in the Arctic Ocean, Global. ⟨https://doi.org/10.1002/(ISSN)1944-9224⟩.
Soerensen, A.L., Mason, R.P., Balcom, P.H., Jacob, D.J., Zhang, Y., Kuss, J., Sunderland, E.M., 2014. Elemental mercury concentrations and fluxes in the tropical atmosphere and ocean. Environ. Sci. Technol. 48, 11312–11319. https://doi.org/10.1021/es503109p.
Soerensen, A.L., Mason, R.P., Balcom, P.H., Sunderland, E.M., 2013. Drivers of surface ocean mercury concentrations and air–sea exchange in the West Atlantic Ocean. Environ. Sci. Technol. 47, 7757–7765. https://doi.org/10.1021/es401354q.
Soerensen, A.L., Sunderland, E.M., Holmes, C.D., Jacob, D.J., Yantosca, R.M., Skov, H., Christensen, J.H., Strode, S.A., Mason, R.P., 2010. An improved global model for air-sea exchange of mercury: high concentrations over the North Atlantic. Environ. Sci. Technol. 44, 8574–8580. https://doi.org/10.1021/es102032g.
St Louis, V.L., Hintelmann, H., Graydon, J.A., Kirk, J.L., Barker, J., Dimock, B., Sharp, M.J., Lehnherr, I., 2007. Methylated mercury species in Canadian high Arctic marine surface waters and snowpacks. Environ. Sci. Technol. 41, 6433–6441. https://doi.org/10.0121/es070692s.
Steffen, A., Bottenheim, J., Cole, A., Ebinghaus, R., Lawson, G., Leaitch, W.R., 2014. Atmospheric mercury speciation and mercury in snow over time at Alert, Canada. Atmos. Chem. Phys. 14, 2219–2231. https://doi.org/10.5194/acp-14-2219-2014.
Steffen, A., Douglas, T., Amyot, M., Ariya, P., Aspmo, K., Berg, T., Bottenheim, J., Brooks, S., Cobbett, F., Dastoor, A., Dommergue, A., Ebinghaus, R., Ferrari, C., Gårdfeldt, K., Goodsite, M.E., Lean, D., Poulain, A.J., Scherz, C., Skov, H., Sommar, J., Temme, C., 2008. A synthesis of atmospheric mercury depletion event chemistry in the atmosphere and snow. Atmos. Chem. Phys. 8, 1445–1482. https://doi.org/10.5194/acp-8-1445-2008.
Steffen, A., Lehnherr, I., Cole, A., Ariya, P., Dastoor, A., Durnford, D., Kirk, J., Pilote, M., 2015. Atmospheric mercury in the Canadian Arctic. Part I: a review of recent field measurements. Sci. Total Environ. 509–510, 3–15. https://doi.org/10.1016/j.scitotenv.2014.10.109.
Stern, G.A., Macdonald, R.W., Outridge, P.M., Wilson, S., Chételat, J., Cole, A., Hintelmann, H., Loseto, L.L., Steffen, A., Wang, F., Zdanowicz, C., 2012. How does climate change influence arctic mercury? Sci. Total Environ. 414, 22–42. https://doi.org/10.1016/j.scitotenv.2011.10.039.
Strode, S.A., Jaeglé, L., Selin, N.E., Jacob, D.J., Park, R.J., Yantosca, R.M., Mason, R.P., Slemr, F., 2007. Air-sea exchange in the global mercury cycle. Glob. Biogeochem. Cycles 21. https://doi.org/10.1029/2006GB002766.
Tekran, 2005. Tekran Model 2537a, Model 1130 Mercury Speciation Unit and Model. Particulate Mercury Unit, User Manuals, Toronto, Canada, pp. 1135.
Tschudi, M., Fowler, C., Maslanik, J., Stewart, J.S., Meier, W., 2016. EASE-Grid Sea Ice Age. Boulder, Colorado USA: NASA National Snow and Ice Data Center Distributed Active Archive Center. ⟨https://doi.org/10.5067/PFSVFZA9Y85G⟩.
Tseng, C.M., Lamborg, C.H., Hsu, S.C., 2013. A unique seasonal pattern in dissolved elemental mercury in the South China Sea, a tropical and monsoon-dominated marginal sea. Geophys. Res. Lett. 40, 167–172. https://doi.org/10.1029/2012GL054457.
U.S. Environmental Protection Agency, 2002. Method 1631, Revision E: Mercury in Water by Oxidation, Purge and Trap, and Cold Vapor Atomic Fluorescence Spectrometry. US EPA Office of Science and Technology, Washington, D.C.
Wang, F., Macdonald, R.W., Stern, G.A., Outridge, P.M., 2010. When noise becomes the signal: chemical contamination of aquatic ecosystems under a changing climate. Mar. Pollut. Bull. 60, 1633–1635. https://doi.org/10.1016/j.marpolbul.2010.05.018.
Zhang, Y., Jacob, D.J., Dutkiewicz, S., Amos, H., Long, M.S., Sunderland, E.M., 2015. Biogeochemical drivers of the fate of riverine mercury discharged to the global and Arctic oceans. Glob. Biochem. Cycles 29, 854–864. https://doi.org/10.1002/2015GB005124.

Further reading

Ci, Z., Zhang, X., Wang, Z., 2011. Elemental mercury in coastal seawater of yellow Sea, China: temporal variation and air-sea exchange. Atmos. Environ. 45, 183–190. https://doi.org/10.1016/j.atmosenv.2010.09.025.
Fantozzi, L., Ferrara, R., Frontini, F.P., Dini, F., 2007. Factors influencing the daily behaviour of dissolved gaseous mercury concentration in the Mediterranean Sea. Mar. Chem. 107, 4–12. https://doi.org/10.1016/j.marchem.2007.02.008.
Sommar, J., Wängberg, I., Berg, T., 2007. Circumpolar transport and air-surface exchange of atmospheric mercury at Ny-Ålesund (79°N), Svalbard, spring 2002. Atmospheric.